PHOTOELECTROCATALYTIC DEGRADATION OF METHYLENE BLUE USING ZNO NANORODS FABRICATED ON SILICON SUBSTRATES

Ana Paula Pereira da Rosa[1‡], Rodrigo Pereira Cavalcante[1‡], Thalita Ferreira da Silva[1], Fábio Gozzi[1], Conor Byrne[2], Enda McGlynn[3], Gleison Antônio Casagrande[1], Silvio César de Oliveira[1], Amilcar Machulek Junior [1**]

(1) Institute of Chemistry, Federal University of Mato Grosso do Sul, Av. Senador Filinto Muller, 1555, CP 549, CEP 79074-460- Campo Grande, MS, Brazil

(2) School of Physical Sciences, Dublin City University, Dublin 9, Ireland.

(3) School of Physical Sciences, National Centre for Plasma Science and Technology, Dublin City University, Glasnevin, Dublin 9, Ireland

[‡]Ana P. P. da Rosa and Rodrigo P. Cavalcante have contributed equally to this work.

[**]Corresponding author:

E-mail addresses: machulekjr@gmail.com (A. Machulek Jr.)

Date of Submission: 11 October 2018

Date of Acceptance: 01 February 2019

Graphic Abstract

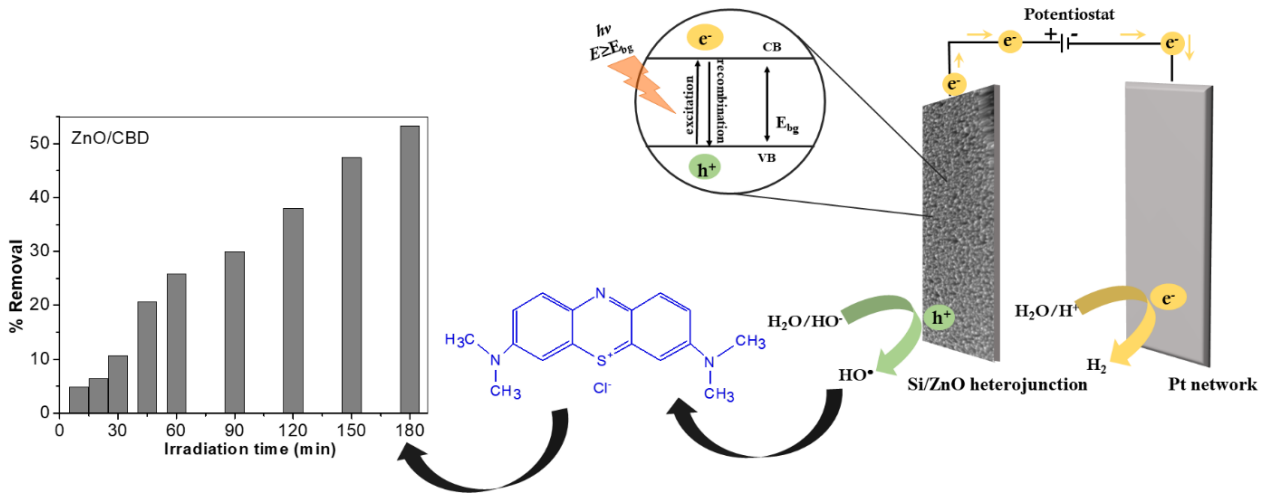

Abstract

ZnO nanorods were grown on silicon (Si) substrates by two techniques: (i) Chemical Bath Deposition (CBD) and (ii) a CBD seed layer combined with Carbothermal Reduction Vapor Phase Transport (CTR-VPT). The structured ZnO nanorods were characterized by scanning electron microscopy (SEM), X-ray diffraction (XRD), X-ray photoelectron spectroscopy (XPS), and contact angle measurments. The photoelectrochemical property of ZnO nanorods were analyzed by linear voltammetry under UV-ABC light excitation. Using the ZnO nanorod samples as photoanodes, the removal of methylene blue (MB) as a representative organic compound was studied by the photoelectrocatalytic (PEC) technique applying a potential (E) of 0.6 V. For comparison purposes, experiments were performed under the same conditions using photocatalysis (PC), direct photolysis and using samples of pure Si (support material) as working electrodes in PEC. XRD analyses of ZnO prepared by both methods showed the expected ZnO wurtzite phase and a preferred c-axial orientation in the growth of the nanorods. The presence of ZnO was further confirmed by XPS and contact angle measurements showed that ZnO grown by CBD (ZnO/CBD) had a slightly hydrophobic behavior while ZnO grown by CTR-VPT (ZnO/CTR-VPT) is hydrophilic. Both ZnO sample types were shown to be photoactive,

with ZnO/CBD showing higher resultant photocurrent compared to ZnO/CTR-VPT. For the degradation of MB 53% of the compound was removed using ZnO/CBD as a working electrode, while using the ZnO/CTR-VPT electrode led to a removal of 43% of MB. However, direct photolysis alone removed 39% of the MB. The lower removal of MB using ZnO/CTR-VPT samples was related to surface dissociation during the degradation process. The results show that ZnO nanorods prepared by the CBD techique are a promising photoelectrode for PEC applications. Our data also indicate that CTR-VPT-grown nanorods produce uniform nanorod arrays, but this uniform nanostructure deposit does not lead to any increase in PEC activity.

Keywords: chemical bath deposition, ZnO nanorods, Si/ZnO heterojunction, photoelectrocatalysis, methylene blue.

1. Introduction

The development of new materials that can be used as semiconductors in photocatalysis (PC) has been the focus of many studies[1]. Trends in photocatalysis research are currently focused on the development of ordered semiconductor nanostructures[2] such as needle-like, nanotubes, nanowires, nanofibers, nanorods, and nanowalls which show higher efficiency due to various factors, including their relatively high surface area and excellent electronic transport properties.[1]

There are many reports in the literature on the use of various semiconductors in PC. Among them, the most extensively studied is titanium dioxide (TiO_2). On the other hand, zinc oxide (ZnO), with a direct bandgap of ~3.3 eV,[3] is an important multi-functional semiconductor, which has clear material advantages such as good photocatalytic activity, low toxicity, high electron mobility, high chemical and thermal

stability, a large optical absorption coeficient, and relatively facile synthesis in various nano-structural forms suitable for a diverse range of applications.[4-7] Therefore ZnO is a promising potential alternative semiconductor material to replace TiO_2, especially for use in photocatalysis.[8-10]

The preparation of different self-organized nanostructures of ZnO on a variety of substrates has attracted much attention to improve the photocatalytic efficiency.[11] The growth of ZnO nanostructures is very sensitive to the synthesis parameters, including temperature, pressure, substrate, and gas flow. One of the main challenges in ZnO nanostructure deposition is control of the synthesis to achieve ordered and uniform growth of a particular desired nano-morphology reproducibly over a suitable substrate area.[11] It is worth mentioning that the larger the area of the material, the more complex is the uniform and reproducible deposition over the entire surface.

ZnO can be grown in various morphology nanostructures, including nanorods,[12] nanobelts,[13] nanosheets,[14] nanotubes,[15] nanoflowers,[16] nanodisks,[17] amongst others. Aligned nanorod arrays, deposited uniformly over substrate areas, are of great interest in the present study for use as a photoanode, due to their large surface to volume ratio, relatively simple synthesis and the enhancement of light absorption due to multiple light scattering among the ZnO nanorods.[18]

These aligned nanorod arrays have been produced using a number of growth methods including chemical bath deposition (CBD),[19] vapour phase transport (VPT),[20] chemical vapour deposition (CVD),[21] carbothermal reduction vapour phase transport (CTR-VPT),[22] electrodeposition,[23] and hydrothermal deposition.[24]

Among these methods, CBD has achieved prominence because of its advantages such as simplicity, controllability, potential for scalable deposition, low cost, and low temperature processing which provides the possibility of using cheap substrates such as

plastics, as well as glass or silicon.[12,25,26] The formation of ZnO nanorods by CBD is explained in detail by Byrne et al.[19]

The use of CBD seed layers in combination with high temperature nanorod growth using carbothermal reduction VPT (CTR-VPT) is an effective route for preparing higher optical quality nanorods.[22] In the present study we grew vertical ZnO nanorod arrays on silicon (Si) substrates using both CBD and CTR-VPT and studied their potential for use as semiconductors in PC and photoelectrocatalysis (PEC).

PEC is extremely attractive for applications concerning oxidization of organic compounds.[27] In comparison to PC, it is highly efficient and sustainable and does not cause secondary pollution.[4] It is based on a semiconductor photoanode that is irradiated by light with energy equal or greater than its band gap and simultaneously with the application of an external bias potential on the semiconductor. When the potential is applied a reduction of the recombination the photo-generated electron-hole pairs occurs and consequently an increase of the PC efficiency is obtained. [28,29]

Nevertheless, at the best of our knowledge, only a few studies are found in the literature using ZnO nanostructures as a photoanode for PEC, including the studies of Hunge et al.[6], Han et al.[30], Liu et al.[31], Lin et al.[32], Suryavanshi et al.[33], and Sarwar et al.[34] These employ nanostructured ZnO as photoanodes for PEC. In addition, only the work of Han et al.[30] used ZnO synthesized by CBD as a photoanode for PEC applications. It is also worth mentioning that, for applications in PEC, no work has been reported in the literature using ZnO grown on (inexpensive and widely available) Si substrates. Hoa et al.[35] fabricated ZnO nanorods on glass and Si substrates by a hydrothermal method and investigated the PC activity of this structure for degradation of Rhodamine B under UV light irradiation. The results indicated that the Si/ZnO nanorod heterojunction exhibits higher photocatalytic activity compared to that of a glass/ZnO nanorod junction. Among

various hybrid forms, when a ZnO/Si heterojunction is formed, photogenerated charge carriers can be separated by an internal electric field and consequently photocarrier recombination is inhibited, contributing to the improvement of PC activity.[35,36] Therefore, further investigations of the Si/ZnO nanorod heterojunction in PEC is a promising area of research, which remains largely unexplored.

The aim of this work is to prepare ZnO nanorods on Si by both the CBD and CTR-VPT methods and to utilise the prepared ZnO deposits for PEC degradation, using methylene blue (MB) as a model organic compound, comparing the efficiency of both the materials synthesised by the two techniques. The crystallinity, surface morphology and PEC performance of the deposited ZnO nanorods were investigated with various techniques such as scanning electron microscopy (SEM), X-ray diffraction (XRD), X-ray photoelectron spectroscopy (XPS), contact angle and linear voltammetry measurements.

2. Material and Methods

2.1.Materials

P-type silicon wafers with a (100) surface orientation were purchased from Wacker-Chemitronic GMBH. Zinc acetate (≥ 99 %) was purchased from Riedel-de Haën. ZnO and graphite, both of high purity (≥ 99.9%) were provided by Alfa Aesar. MB (97% pure) was purchased from Dinâmica do Brasil. The other reagents and solvents (purchased elsewhere) were used as received. Deionized water was used in all experiments.

2.2.Synthesis of ZnO nanorod arrays

ZnO nanorods were grown on silicon (Si) substrates by two techniques: (i) CBD and (ii) CTR-VPT. Both procedures were based on the reports of Byrne et al.[19,22]

2.2.1. Chemical Bath Deposition (CBD)

Silicon (100) wafers were cleaved into small rectangles with an area of 6.5 cm^2, and were then cleaned by sonication in ethanol and dried in a nitrogen stream.

First, a thin ZnO seed layer was formed on the substrate. For this, 24.375 μL of a 5 mmol L^{-1} zinc acetate solution prepared in absolute ethanol was deposited by drop coating on the center of the substrate. This amount is equivalent to 3.75 μL of zinc acetate per cm^2 of substrate, according to the previous studies of Byrne et al.[22] The zinc acetate solution was allowed to remain on the substrate surface for 20 s, thus allowing the solution to spread over the entire substrate. After this step, the material was rinsed with a copious amount of ethanol and dried with nitrogen. The zinc acetate coating procedure was performed five times consecutively in each sample, and thereafter the substrate containing zinc acetate was annealed in atmospheric air at 350 °C for 30 min.

The next step was to prepare the chemical bath. For this procedure,[19] 100 mL of a 0.02 mol L^{-1} zinc nitrate solution was slowly added to 100 mL of a 0.8 mol L^{-1} NaOH solution with vigorous stirring. This mixture was heated to 70 ºC and ZnO seeded substrates were submerged into the solution and maintained at this controlled temperature with stirring for 25 minutes. Subsequently, the substrates were removed from the bath, washed with deionized water and dried with a nitrogen stream.

2.2.2. Carbothermal reduction vapour phase transport deposition (CTR-VPT)

In this procedure, 0.06 g of ZnO powder was mixed with an equal mass of graphite until they formed a homogeneous gray powder and this was then distributed evenly into an alumina boat. The substrates containing ZnO nanorods deposited by the CBD technique described above (which are now used as a seed layer for CTR-VPT growth) were placed directly over the graphite/ZnO mixture (in identical symmetrical positions) so that when it was placed in the furnace, the vapors from the mixture rise directly onto the CBD ZnO nanorod covered Si surface. The boat containing the substrate was then placed inside a quartz tube and positioned at the centre of a horizontal single zone tube furnace and was heated at 900 °C under a 100 sccm argon flow and maintained at this temperature for 1 h. After this period, the material was cooled to room temperature and removed from the furnace. A schematic diagram of the ZnO nanorod synthesis procedure is given in Figure 1.

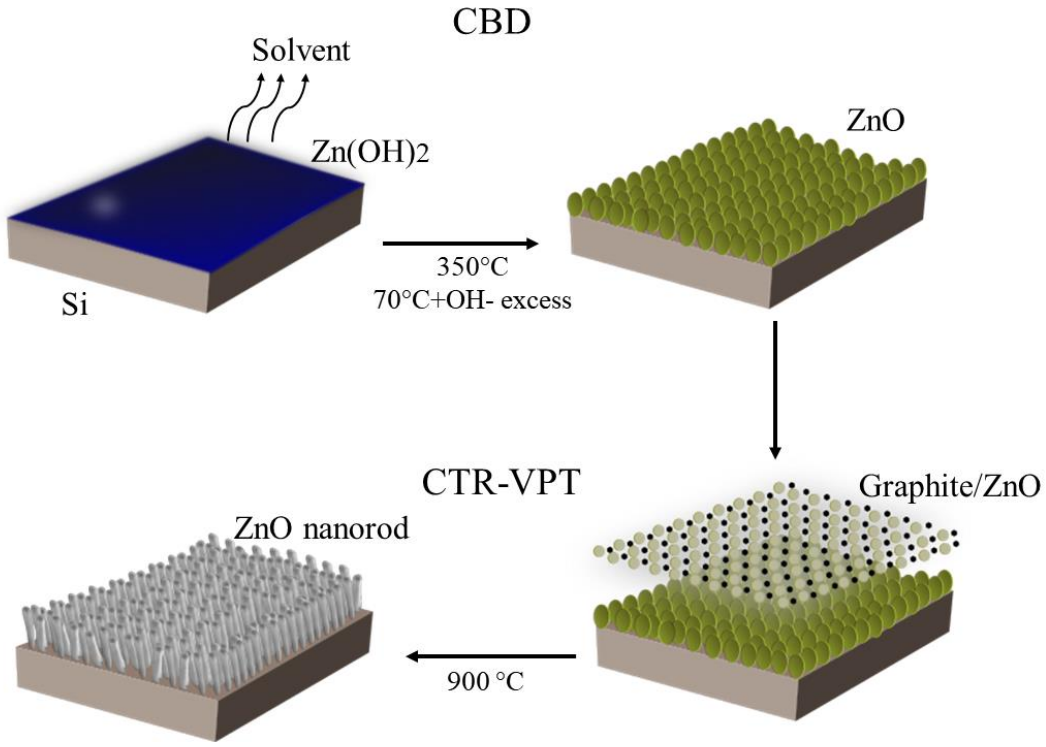

Figure 1: Schematic representation of growth mechanisms of ZnO nanorods in the CBD and CTR-VPT processes, showing the formation of the p-Si/n-ZnO heterojunction.

2.3.Characterization

The morphologies of the deposits were examined using SEM (Karl-Zeiss EVO series). The crystal phases of the synthesized samples were determined by XRD analysis using a Brucker AXS D8 Advance Texture Diffractometer with CuKα radiation (λ = 1.541874 Å) over the 2θ range 10–80º. Material surface composition was analyzed by XPS using a VG Microtech electron spectrometer at base pressure of 1×10^{-9} mbar using a conventional Al Kα (hν = 1486.7 eV) x-ray source. The pass energy of the analyser was set at 20 eV, yielding an overall resolution of 1.2 eV. All peak analysis presented in this study was performed using AAnalyzer curve fitting software program version 1.20. The calibration of the binding energy scale was performed with the C1s line (285 eV) from the adventituous carbon contamination layer.

Contact angle (CA) measurements were performed using an FTA-200 contact angle analyzer (First Ten Angstroms, USA) by imaging a droplet of water that was dispensed onto the ZnO nanorod deposit surface. The average CA for distilled water was determined in a progression of ten estimates for each electrode. The captured images were then analysed using FTA32 software.

The linear scan voltammetry plots for measuring photocurrents in order to analyze the photoactivity of the synthesized ZnO electrodes were carried out using a VersaStat II potentiostat/galvanostat (Princeton Applied Research) controlled via Echem software using a three-electrode configuration with a Pt network counter electrode, a Ag/AgCl/KCl 3 mol L^{-1} reference electrode, and the synthesized ZnO electrodes as working electrodes. The working electrode was 6.5 cm^2 in active area. The parameters of voltammetry were as follows: potential range = - 0.5 to + 3.5 V; equilibrium time: 15 s; scanning speed: 5 m Vs^{-1}. The electrolyte was 0.05 mol L^{-1} Na_2SO_4 solution. The photoresponse of the ZnO electrodes were measured as UV-ABC radiation source using an 80 W HPL-N, high-pressure mercury vapor lamp (222-578 nm, with maximum emission at 254 nm, Orsan) at a flux of $3.71x10^{19}$ photons s^{-1} experimentally determined by chemical actinometry.[37] The system was kept under constant stirring and the lamp was immersed in the 350 mL electrolyte solution inside a quartz tube with water inlet and outlet, allowing cooling of the system (keeping the working solution at ~ 25ºC) with the aid of a thermostatic bath.

2.4.PEC degradation

The PEC activity of the ZnO photoelectrodes was evaluated by degrading MB solution under UV-ABC irradiation (the same lamp used to investigate the photoresponse of the ZnO electrodes, see details above). The photoelectrodegradation experiments were carried out in a PEC reactor, composed of three electrodes: a Pt network as counter

227 electrode, ZnO nanorods synthesized by the CBD technique and/or ZnO nanorods grown
228 by the CTR-VPT technique as working electrodes and a Ag/AgCl/KCl 3 mol L^{-1}, as the
229 reference electrode. The reactor was filled with an aqueous solution of 20 mg L^{-1} of MB
230 prepared in 350 mL of Na_2SO_4 (0.05 mol L^{-1}). A positive bias potential of 0.6 V[32] was
231 applied by a potentiostat (VersaStat II), for a period of up to 180 min. The schematic of
232 the PEC reactor used is illustrated in Figure 2.

233 For comparison, a PEC experiment was also conducted using samples of pure p-
234 type Si (the support material) as working electrodes, as well as an experiment using direct
235 photolysis and experiments using only PC, without application of an external potential.
236 All control experiments were performed under the same conditions described above.

237 The the conversion rate was examined by measuring the absorbance of the MB at
238 664 nm on a Unicam UV–Vis spectrophotometer. To monitor MB concentration, a
239 calibration curve was obtained in the 0.25-25 mg L^{-1} range, with Abs (a.u.) = 0.0027 +
240 0.12813 [MB, mg L^{-1}]; R = 0.999, SD = 0.024.

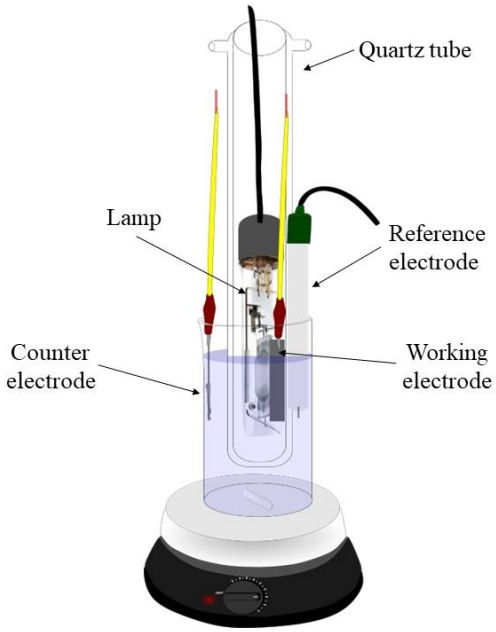

241

242 **Figure 2:** Scheme of the PEC reactor composed of three electrodes.

243

3. Results and Discussion

3.1.Characterization results

Samples obtained using both methods of ZnO synthesis gave rise to nanorods on the Si substrates. Figure 3 shows SEM images of ZnO nanorod films deposited by CBD for three different samples. Figures 3(a) and (b) show plan and cross-sectional views for one sample (labelled C1). From these images we clearly observe well-aligned ZnO nanorod arrays with uniform diameters and uniform coverage over the Si substrate. The morphology of samples C2 and C3 are shown in Figures 3(c) and (d) and reveal that the nanorods are less obviously distinct and more densely packed.

Slight variations in morphology between samples of the sort seen in Figure 3 were also observed by Maryam et al.[38] in a study of synthesis of ZnO nanorods on glass substrates. The differences are quite minor and are likely due to small variations in the deposition of the initial seed layer of ZnO deposited by drop coating, a step that proved to be very important for obtaining well-defined ZnO nanorods by the CBD techique.

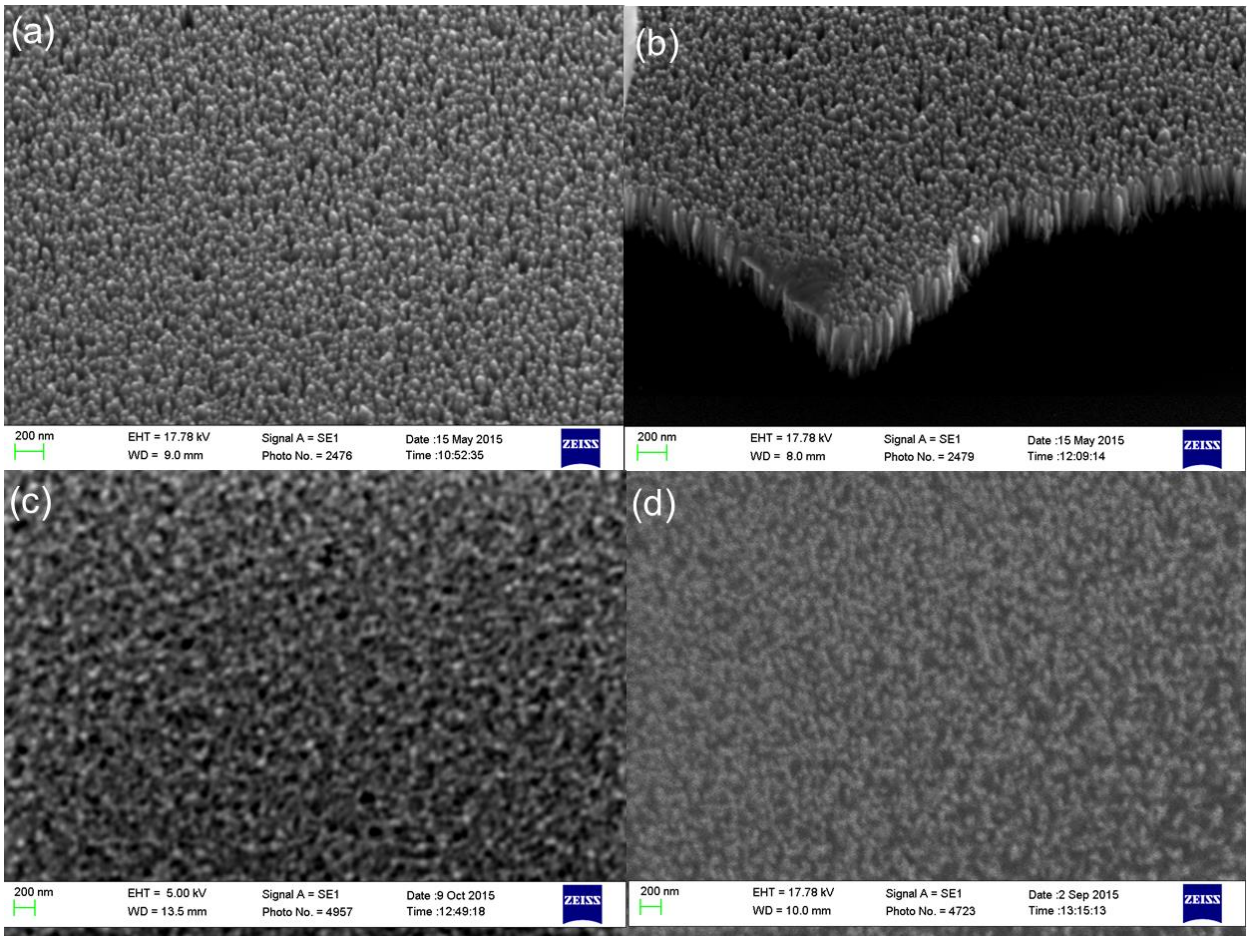

Figure 3: SEM images of the ZnO nanorods grown by the CBD method showing (a) a plan view and (b) a cross-sectional view of sample C1 and plan views for samples C2 (c) and C3 (d).

Following CBD deposition, CTR-VPT growth was performed on some samples. Figure 4 shows plan and cross-sectional view SEM images of ZnO nanorods films after CTR-VPT growth. The CTR-VPT step produced longer narrow, well-aligned ZnO nanorods with more uniformly diameters a top the original CBD seed layer.

As can be seen in Figure 4, the ZnO nanorods are uniformly distributed on the Si substrates. The average diameter of ZnO/CTR-VPT nanorods at the center of the sample is 158 ± 25 nm and their average height is 4.7 ± 0.4 µm. At the edges of the ZnO arrays the average diameter is 227 ± 68 nm and the average height is 1.6 ± 0.2 µm.

The rods are narrower and longer in the center of the sample and, as they approach the edges, they become wider and shorter. These variations of the size of the ZnO nanorods likely result from a variation in supersaturation of the Zn^{2+} growth species during the synthesis process, as has been reported previously.[39]

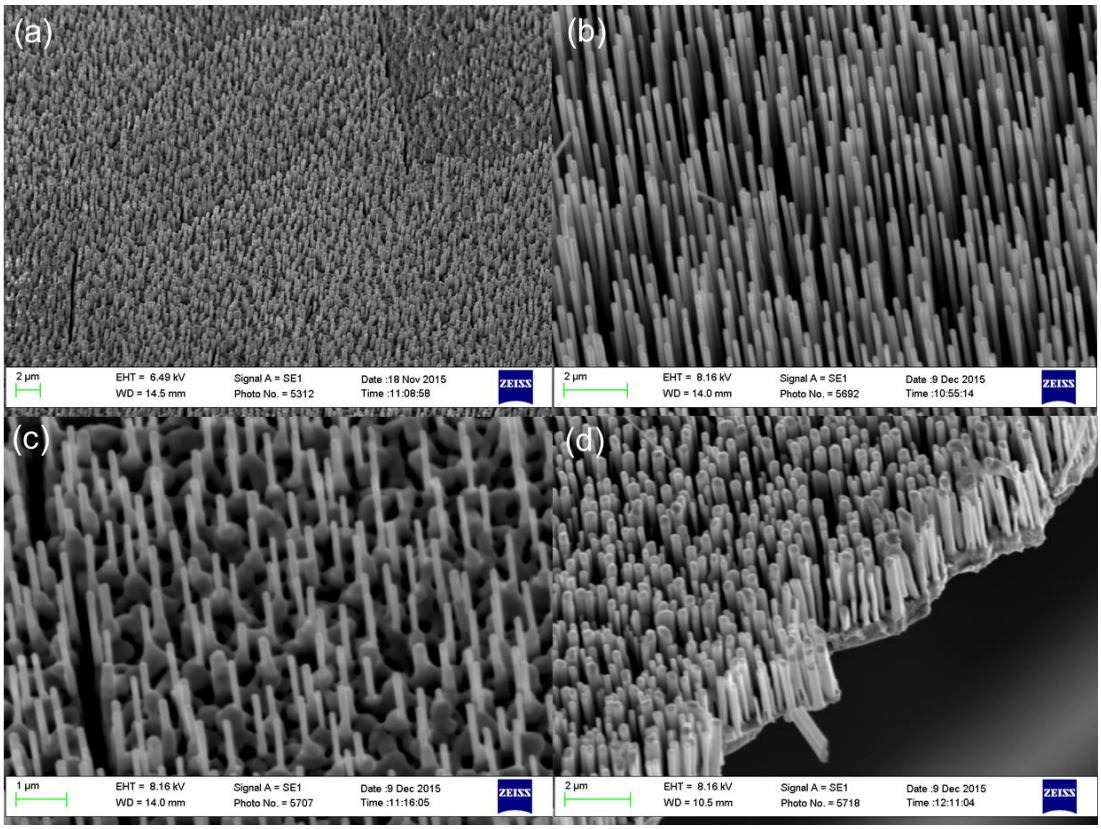

Figure 4: SEM images of the ZnO nanorods grown by CTR-VPT. (a) Plan view and (b-d) 30 º view.

Figure 5 shows XRD results for the deposited ZnO nanorods grown by both methods. The predominant diffraction peaks observed at a 2θ value of 34.45º correspond to reflections from (002) planes of wurtzite hexagonal ZnO.[40-42] No diffraction peaks corresponding to metallic Zn were found in any region of the electrode. This sharp and dominant (002) diffraction peak indicates the nanorods are well crystallized and highly oriented with their c-axes orientation normal to the substrate surface.[43,44] The intense peak

located at 69.15° corresponds to the Si peak from the (004) Si planes used as the substrate.[45,46]

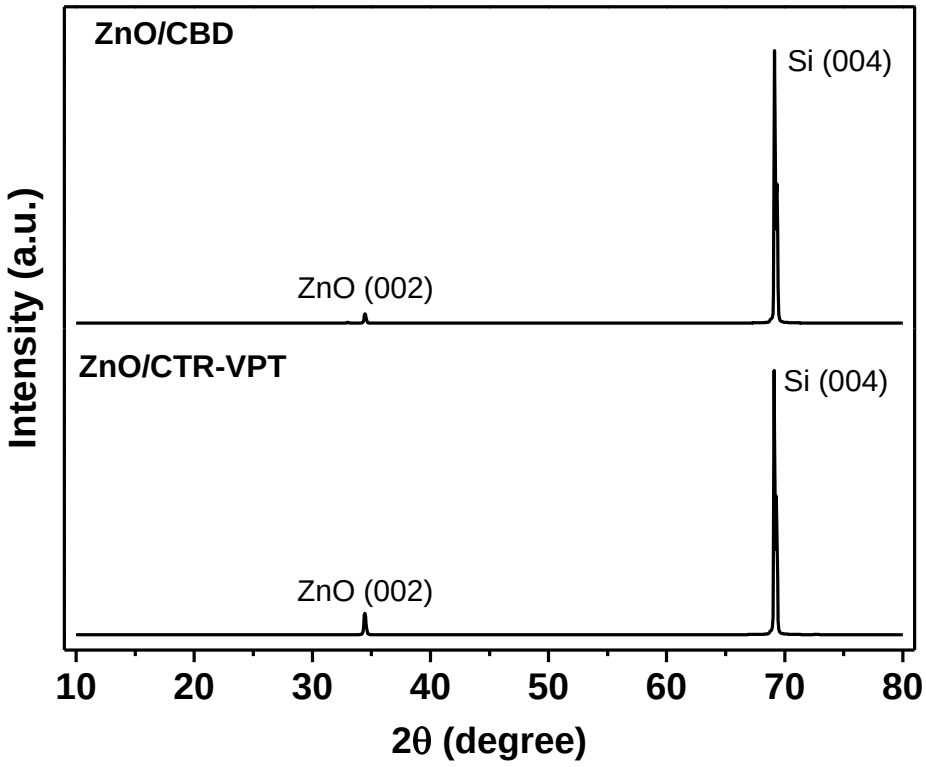

Figure 5: XRD patterns of ZnO nanorod arrays grown on silicon, displaying two dominant peaks, associated with the ZnO (002) and Si (004) reflections, at 34.41º and 69.15º, respectively.

In order to observe the low intensity peaks in the diffractogram, the spectra was plotted on a logarithmic y-scale.[47] Figures 6(a) and (b) shows the XRD diffractograms of the ZnO/CBD and ZnO/CTR-VPT samples on a logarithmic y-scale. It can be observed that in addition to the two most intense peaks at 34.45º and 69.15º, there are reflections from the (004) and (100) planes of ZnO[45] for the samples synthesized by both methods, as well as the nominally forbidden Si(002) reflection for the sample synthesized by CBD method, due to double diffraction, whose intensity depends on the azimuthal angle, ϕ ,

and which hence is not seen with equal intensity in all samples.[48] Some small peaks, labelled as F, are also observed and are attributed to the adhesive tape used to mount the samples at the time of analysis. Gray et al.[45] also report the presence of the same F peaks. According to the studies of Gray et al.[45] and Kumar et al.[49] the point marked as X is due to *Kβ* radiation at ~ 61.7º from the X-ray tube and the feature marked as Y is due to tungsten *L*α radiation at ~ 65.7º from contamination of the x-ray tube Cu target by the electron gun filament. No other peak-related impurities were observed in the pattern which confirms the presence of pure wurtzite phase ZnO nanostructures.

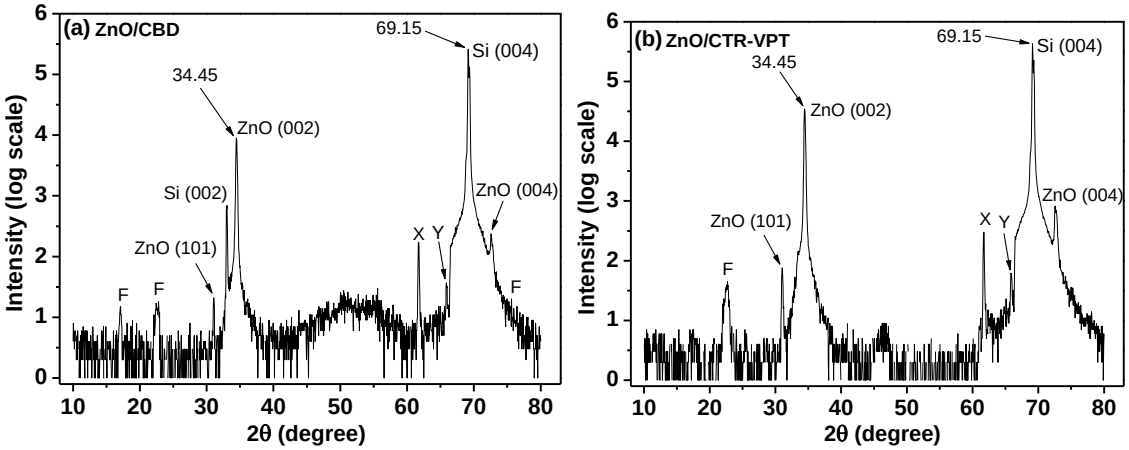

Figure 6: XRD patterns of ZnO samples on a logarithmic y-scale, to enhance the visibility of low intensity peaks.

Figure 7 shows the results of XPS measurements of ZnO nanorods. Figures 7(a) and (c) show XPS survey spectra of the samples grown by CBD and CTR-VPT, respectively, confirming the presence of elements Zn, O and C. No other elements are seen. The presence of C is due to atmospheric contamination (seen on all samples exposed to ambient conditions). Thus, the results confirm the high purity of the ZnO nanorods and is in accordance with the XRD analysis.

322 Figures 7(b) and (d) shows the Zn 2p core level emissions from ZnO nanorods
323 grown by CBD and CTR-VPT, respectively. For the ZnO/CBD sample, the doublets
324 corresponding to the $2p_{3/2}$ and $2p_{1/2}$ photoelectron core level peaks are centrally
325 positioned at 1022.8 eV and 1046 eV, respectively, in the spectrum. In case of ZnO/CTR-
326 VPT the electronic states of Zn $2p_{3/2}$ and Zn $2p_{1/2}$ were observed at the binding energies
327 of 1022.9 eV and 1045.9 eV, respectively. These values agree within the energy
328 resolution of the system. For the ZnO/CBD sample the binding energy distance between
329 the two spin orbit split peaks is 23.2 eV while in case of ZnO/CTR-VPT sample the spin
330 orbit separation is 23 eV, again in agreement within the system's energy resolution, and
331 demonstrating that the Zn species exist in the Zn^{2+} chemical state, consistent with
332 previous work in the literature and with reference data for ZnO.[50-53]
333
334

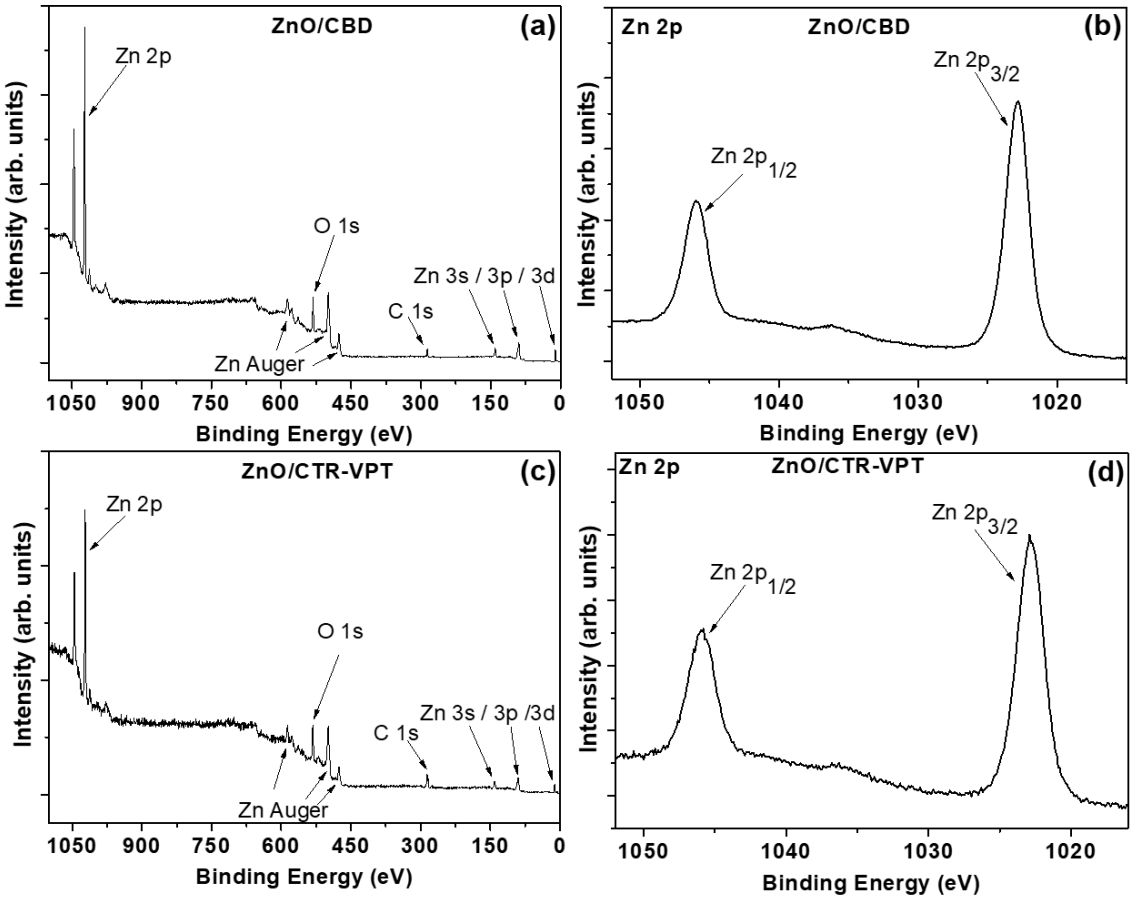

Figure 7: XPS spectra for the ZnO/CBD (a, b) and ZnO/CTR-VPT samples (c, d). (a, c) XPS survey spectra, (b, d) high resolution Zn 2p XPS spectrum.

Figure 8 shows the XPS spectra in the O 1s region for the ZnO/CBD sample. The O 1s signal can be deconvoluted into two Gaussian peaks, at binding energies of 531.6 eV and 533.04 eV, commonly called O(1) and O(2), respectively. The peak at the lower binding energy is assigned to O^{2-} ions in the O-Zn bonding matrix of the hexagonal ZnO wurtzite structure.[50,52-56] The other peak at the binding energy of 533.04 eV is associated with O^{2-} that is present in the oxygen deficient regions[53,57] or OH species on the surface of ZnO nanorods.[52,55,58]

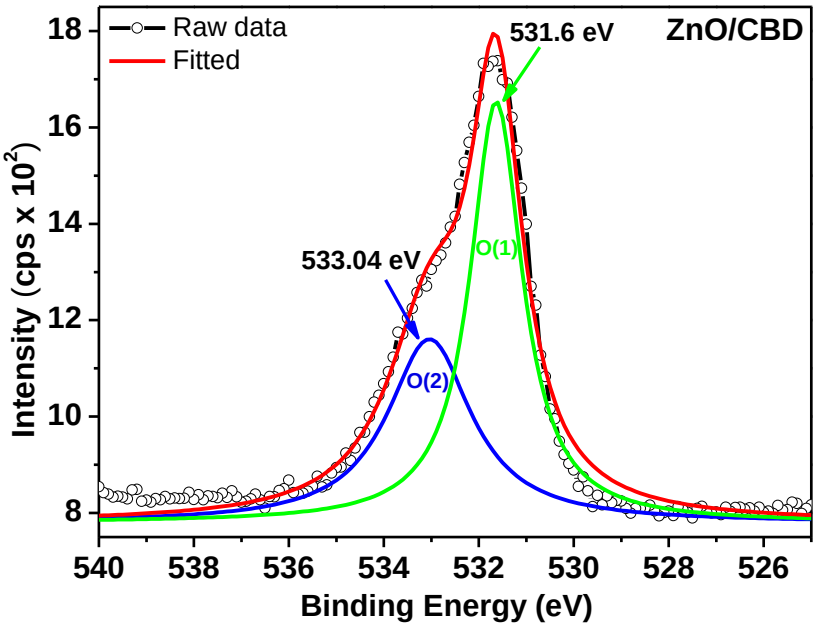

Figure 8: Oxygen 1s XPS spectra of ZnO nanorods grown by CBD.

To investigate the wettability of the ZnO nanorods, a water CA measurement was carried out.[59,60] The ZnO nanorod arrays grown by CBD showed the highest water contact angle of about 92° ± 4°. In contrast, ZnO/CTR-VPT samples show water contact angle of 64° ± 8°, indicating an increase in the hydrophilicity.[61] The wettability is an important property of solid surfaces that depends on the chemical composition, energetics and geometric surface structures. In this case, ZnO/CTR-VPT samples have a lower contact angle, possibly due to their well-organized, and quite long, nanorod morphology, leading to greater hydrophilicity.[26,60]

Figures 9(a) and (b) show the photocurrent densities of ZnO/CBD and ZnO/CTR-VPT photoanodes operating under dark and illuminated conditions. The results indicate that ZnO nanorod arrays formed by both techniques respond to UV-ABC irradiation. The current response of both films in the dark is very weak. However, when the experiment is performed under illumination, the current increases strongly, showing that synthesized ZnO nanorods are a good photocatalyst for PEC.[5] It can be seen that UV-ABC irradiation

364 obviously increases the current when the potential is higher than 0 V. This is attributed to
365 photogenerated electrons on the ZnO nanorods driven to the counter electrode by the
366 application of a positive potential. Thus, the recombination of the photogenerated
367 electron–hole pairs is hindered and increased photocurrent is generated.[5,18]

368 The photocurrent density of the ZnO nanorods prepared by CBD was observed to
369 be highest (~ 0.87 mA cm^{-2} at +3.5 V); it was about two hundred times that of the
370 ZnO/CTR-VPT sample at +3.5 V. This result indicates that the ZnO nanorod arrays
371 prepared by CBD possess excellent PEC response under UV illumination.

372 Due to the fact that ZnO grown by CTR-VPT presented a morphology with more
373 organized nanorods, it was initially expected that these samples would present better
374 charge transport, leading to a higher photocurrent density. However, the photocurrent
375 across the ZnO/CBD sample is much higher. The enhancement of the photocurrent of the
376 ZnO/CBD photocatalyst compared to ZnO/CTR-VPT samples may have a number of
377 origins. Firstly the higher growth temperatures used for CTR-VPT growth can lead to an
378 increased thickness SiO_2 layer between the Si and ZnO, retarding current flow.[62] A further
379 contribution may come from heterojunction formation between the p-Si (substrate) and
380 the CBD ZnO layer with lower thickness; thus, when the p-Si and the n-ZnO make
381 electrical contact with each other their Fermi levels will equalise, leading to the shift of
382 their conduction and valence bands;[35] Another possible source for the lower photocurrent
383 of the ZnO/CTR-VPT sample is the presence of defects on surface of the ZnO/CTR-VPT,
384 which may lead to relatively low efficiency separation of the photogenerated carriers.[60]
385 XPS data presented previously indicate slight differences in surface chemistry between
386 the CBD and CTR-VPT samples.

387

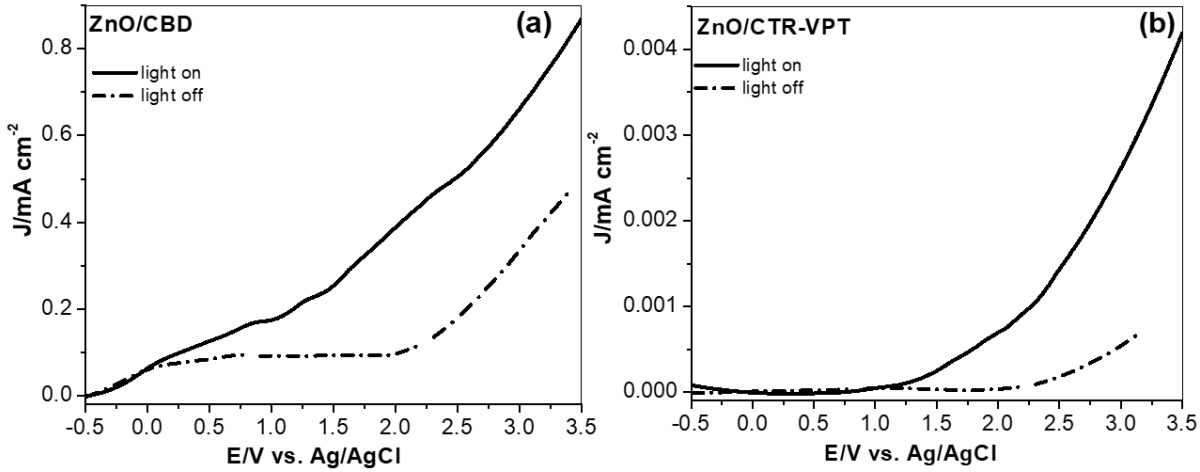

388

389 **Figure 9:** Current density-voltage curves of the ZnO nanorod samples in the dark and
390 under UV-ABC irradiation recorded in a 0.05 mol L^{-1} Na_2SO_4 electrolyte at a
391 scan rate of 50 mV s^{-1}.

392

393 *3.2.Investigation of PEC efficiency of ZnO nanorods*

394 The PEC degradation of MB solution under UV-ABC light irradiation was used
395 to evaluate the PEC activities of ZnO/CBD and ZnO/CTR-VPT electrodes under the
396 experimental conditions indicated previously. The results of degradation experiments are
397 shown in Figure 10(a). About 43% of MB was degraded in 180 min when the ZnO/CTR-
398 VPT electrode was used for the PEC process, while it improved to 53% when using the
399 ZnO/CBD photoelectrode. By comparison, the removal rate using the PC technique is
400 only 41% and 39% using ZnO/CBD and ZnO/CTR-VPT, respectively.

401 As mentioned in the introduction, Han et al.[30] prepared ZnO nanorod arrays on
402 Ag by CBD and evaluated the PEC performance of the electrode for the removal of
403 rhodamine B (RhB). Applying a potential of 0.4 V and using 0.1 mol L^{-1} of Na_2SO_4 as
404 support electrolyte, the authors obtained 38% RhB removal after 5 h of treatment. This
405 study demonstrates that our results are comparable with those found in the literature for
406 similar morphology ZnO nanomaterials.

Figure 10(b) shows the variation in the absorption spectra from 200 to 800 nm of MB collected at different time intervals during the PEC degradation experiment using a ZnO/CBD sample as a catalyst. The absorption spectrum of MB shows two peaks of lower intensities at 246 and 292 nm and a more intense peak at 664 nm. The peaks at 246 and 292 nm are due to the substituted benzene ring structures while the peak at 664 nm is attributed to the auxochrome group of MB.[63] It can be seen that the absorbance peaks decreased gradually as the exposure time increases from 0 to 180 min. The visual appearance of the MB solution changed from dark blue to nearly colourless over this period.

A control experiment was conducted by studying the degradation of this dye under UV-ABC irradiation in the absence of electrodes. In this case, about 39% removal of MB was obtained. As a comparison, the PEC process using bare Si as the working electrode was also carried out in order to verify the influence of the substrate in the degradation of the MB. This blank experiment showed that the degradation rate is 36% in 180 min. It is observed that the degradation rate was lower than that found in direct photolysis, indicating that the PEC activity of Si can be neglected. One hypothesis to elucidate the lower degradation rate in the presence of Si compared to direct photolysis would be that MB molecules adsorb on the surface of the material and remain adsorbed due to the low conductivity of the pure Si and the insulating native oxide (SiO_2).

The degradation rates of MB were analysed using the Langmuir–Hinshelwood pseudo-first order kinetics model. Following this model, the degradation rate constants (k_{ap}) are calculated from the linear fit extracted from the $-\ln(C/C_0)$ vs. Time data (Figure 9(c)). As shown in Figure 10(c), the magnitude of k_{ap} shows the following ordering; ZnO/CBD > ZnO/CTR-VPT = direct photolysis > pure Si. It is apparent that the kinetic constant of PEC using a ZnO/CBD photoelectrode is the highest, and is 1.4 times more

effective than PC.

Comparing the processes of direct photolysis and PEC degradation using a ZnO/CTR-VPT electrode as catalyst, it can be seen that there was no significant difference in the degradation rate of the MB, which shows that the synthesized ZnO does not demonstrate PEC activity under the applied conditions. The low photoactivity of this electrode in comparison to the electrode grown by CBD is due to the low current density seen in the potential photocurrent curves (Figure 10(b)), ~ 4.18 μA cm^{-2} at 3.5 V. SEM images of the ZnO/CTR-VPT surface before (Figure 4) and after (Figure 11) the PEC process show that the applied potential may also have caused a physical degradation of the surface of the oxide, leading to a further reduction of its photocatalytic activity.

Other factors may also have influenced the PC and PEC responses, leading to improved results for ZnO/CBD electrodes compared to ZnO/CTR-VPT electrodes. The results of CA measurements, show that the ZnO/CBD electrode presented a higher contact angle, consequently it presents a greater wettability, which may lead to a better interaction between the surface and working solution and, consequently higher production of hydroxyl radicals ($HO^{\bullet}$), increasing the photocatalytic response. SEM images show that the CBD-grown nanorods are smaller and consequently the surface area is larger; it is well known that a photosemiconductor with a relatively larger surface area in general tends to show better catalytic response.

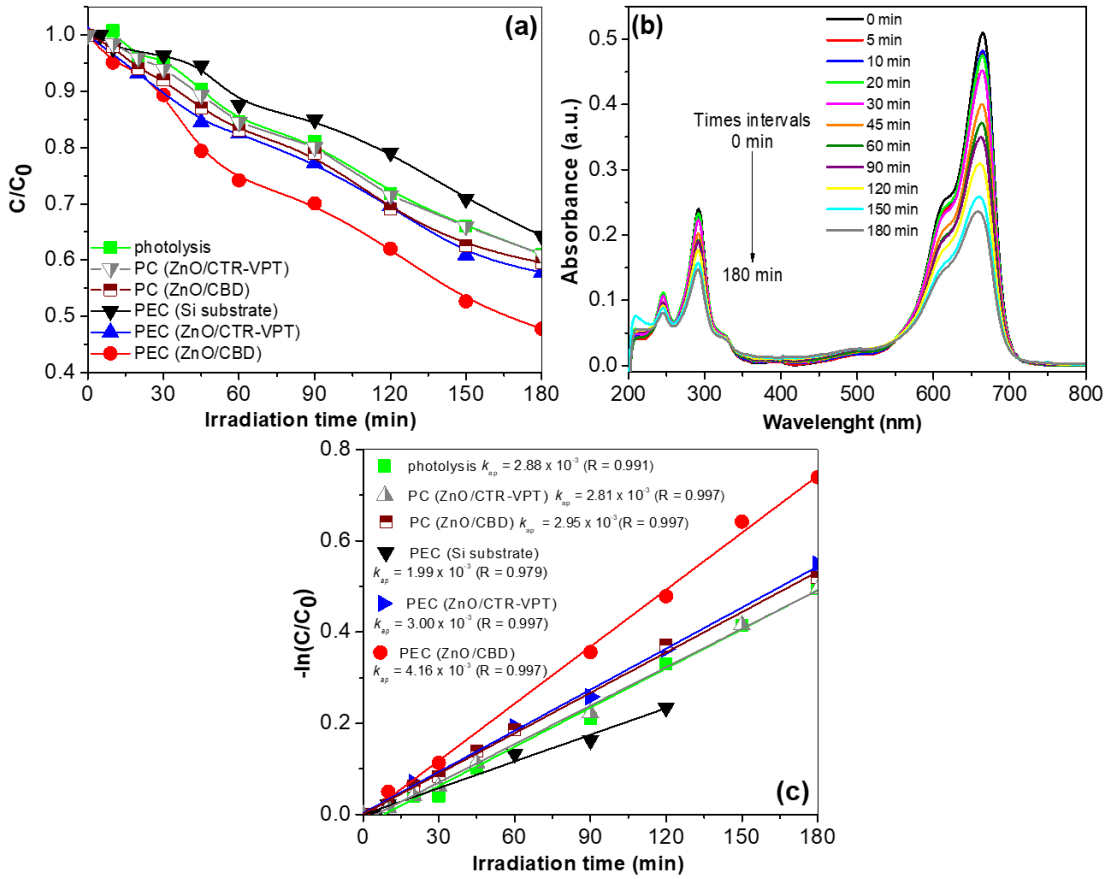

Figure 10: (a) MB degradation curves under UV-ABC irradiation; (b) Absorbance spectra of MB with respect to time subjected to PEC treatment with ZnO/CBD electrode at 0.6 V; (c) Corresponding kinetics fitting curves.

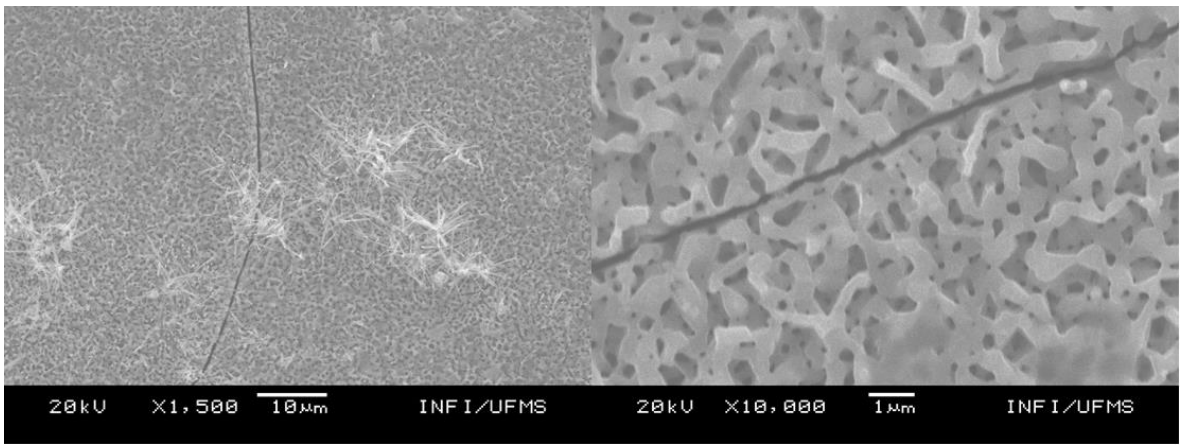

Figure 11: SEM images of ZnO nanorods grown by CTR-VPT after the PEC process.

As mentioned in the introduction, there are few reports of the application of ZnO nanorods for PEC degradation of contaminants compared to TiO_2. We now discuss the reports mentioned in the introduction in more detail, in order to allow direct comparison with our results. Fan et al.[5] evaluated the efficiency of ZnO films deposited on titanium plates by liquid phase deposition (LPD) as photoanodes for the removal of p-nitrophenol by PEC. The authors obtained 91% of p-nitrophenol removal after 180 min of irradiation in optimized conditions. Hunge et al.[6] synthesized ZnO thin films on glass and fluorine doped tin oxide (FTO) coated glass substrates by spray pyrolysis and evaluated the efficiency of these electrodes for PEC degradation of terephthalic acid. The degradation percentage of terephthalic acid using ZnO photoelectrode reached up to 91% under ultraviolet illumination after 400 min. Liu et al.[31] synthesized CdS-Coated ZnO nanorods arrays by a two-step method. Firstly, ZnO nanorod arrays were grown under hydrothermal conditions on an ITO substrate and secondly, a coating of CdS on the surface of the ZnO was realized by a successive ionic layer adsorption and reaction (SILAR) method and the authors then evaluated the efficiency of the photoanodes for PEC degradation of phenol. In the PEC process, about 80% degradation of 100 mg L^{-1} phenol solution is achieved within 150 min under visible light irradiation. Lin et al.[32] evaluated the PEC degradation of paracetamol using ZnO nanorod-array electrodes on FTO glass via a hydrothermal method. The authors obtained 62% paracetamol removal after 20 hours. Suryavanshi et al.[33] prepared ZnO thin films on glass and FTO coated glass substrates by spray pyrolysis and evaluated the efficiency of these electrodes for PEC degradation of of benzoic acid (BA) and methyl blue (MB) dye under UV radiation. The results of this study showed 65.7% degradation of BA and 98.1% of MB within 400 min and 120 min, respectively. Sarwar et al.[34] investigated the removal of textile dyeing effluents with voltage-assisted PC activity using carbon fabrics containing ZnO nanorods as photoanodes. In this study,

ZnO nanorods were grown by a seeding technique followed by a hydrothermal process. The study concludes that carbon fabric treated with ZnO nanorods can be successfully utilized for enhanced decolorization of dye contaminated wastewater, providing an environmental friendly solution for the treatment of effluents generated by textile, leather and other industries. Our results are consistent with these literature reports and allow us to claim that ZnO nanorods deposited on Si substrates by CBD show good potential for use as a working electrode in PEC, and that the use of Si substrates, in addition to the facile CBD synthesis process provides some advantages compared to the other methods described in terms of scalability and cost.

4. Conclusions

In this study, we successfully fabricated well-aligned ZnO nanords on Si with a geometrical area of ~ 6.5 cm^2 by CBD and CTR-VPT.

The ZnO nanorods synthesised have a hexagonal wurtzite structure and are textured normal to the substrate surface, as shown by XRD and SEM data. The nanostructures synthesized by CTR-VPT resulted in a more organized structure with narrower and longer nanorods.

XPS data indicated the presence of pure ZnO deposited on the Si substrate, while contact angle measurements revealed that nanorods synthesized by CTR-VPT have greater wettability compared to ZnO synthesized by CBD. The photoactivity of ZnO/CBD is larger than that of ZnO/CTR-VPT. After 180 min illumination, the PEC degradation of MB concentrations using ZnO/CBD reached 53%, about 1.2 times that of ZnO/CTR-VPT samples. The degradation process follows pseudo-first order kinetics and k_{ap} values have been extracted.

This work demonstrates that more ordered ZnO nanorods were not the best morphology for applications in PEC, and we show that the CTR-VPT process does not produce ZnO nanorods optimised for applications in PEC. The simpler and less expensive CBD technique by itself produces samples which show better performance for PEC applications and which are also more chemically robust.

Acknowledgments

The authors thank the Brazilian funding agencies Conselho Nacional de Desenvolvimento Científico e Tecnológico (CNPq), Coordenação de Aperfeiçoamento de Pessoal de Nível Superior (Capes, Finance Code 001), Fundação de Apoio ao Desenvolvimento do Ensino, Ciência e Tecnologia do Estado de Mato Grosso do Sul. The authors acknowledge financial support under the Irish Research Council Enterprise Partnership Scheme in partnership with Intel Ireland, in addition to financial support from Science Foundation Ireland under the SFI PI award 13/IA/1955. The authors would like to thank the Drs. Ciaran Gray and Saikumar Inguva for their kind help and support during APPdR's research period in the School of Physical Sciences, Dublin City University.

References

1. G. G. Bessegato, T. T. Guaraldo, J. F. de Brito, M. F. Brugnera, and M. V. B. Zanoni, *Electrocatalysis* 6, 415 (**2015**).

2. F. Bakhshandeh, A. Azarniya, H. R. M. Hosseini, and S. Jafari, J. *Photochem. Photobiol. A. Chem.* 353, 316 (**2018**).

3. M. A. M. Ahmed, B. S. Mwankemwa, E. Carleschi, B. P. Doyle, W. E. Meyer, and J. M. Nel, *Mater. Sci. Semicond. Process.* 79, 53 (**2018**).

4. J. Feng, L. Cheng, J. Zhang, O. K. Okoth, and F. Chen, *Ceram. Int.* 44, 3672 (**2018**).

5. M. Fan, C. Yang, W. Pu, and J. Zhang, *Mater. Sci. Semicond. Process.* 17, 104 (**2014**).

6. Y. M. Hunge, A. A. Yadav, S. B. Kulkarni, and V. L. Mathe, *Sens. Actuators. B. Chem.* 274, 1 (**2018**).

7. R. N. Gayen, and R. Paul, *Nano-Structures & Nano-Objects* 13, 163 (**2018**).

8. D. D. Ramos, P. C. S. Bezerra, F. H. Quina, R. F. Dantas, G. A. Casagrande, S. C. Oliveira, M. R. S. Oliveira, L. C. S. Oliveira, V. S. Ferreira, S. L. Oliveira, and A. Machulek Jr., *Environ. Sci. Pollut. Res. Int.* 22, 774 (**2015**).

9. R. P. Cavalcante, R. F Dantas; B. Bayarri, O. González, J. Giménez, S. Esplugas, and A. Machulek Jr., *Catal. Today*. 252, 27 (**2015)**.

10. P. C. S. Bezerra, R. P. Cavalcante, A. Garcia, H. Wender, M. A. U. Martines, G. A. Casagrande, J. Giménez, P. Marco, S. C. Oliveira and A. Machulek Jr., *J. Braz. Chem. Soc.* 28, 788 (**2017**).

11. E. Mcglynn, M.O. Henry, J.-P. Mosnier, in *The Oxford Handbook of Nanoscience and Technology* edited A.V. Narlikar and Y.Y. Fu, Oxford Handbooks Online, (**2017**)

Vol. 2, p. 522.

12. Z. Zheng, J. Lin, X. Song, and Z. Lin, *Chem. Phys. Lett.* (**2018**), doi: https://doi.org/10.1016/j.cplett.2018.09.006

13. X. Qu, S. Lu, J. Wang, Z. Li, and H. Xue, *Mater. Sci. Semicond. Process.* 15, 244 (**2012**).

14. K. Sahu, S. Choudhary, J. Singh, S. Kuriakose, R. Singhal, and S. Mohapatra, *Ceram. Int.* (**2018**), https://doi.org/10.1016/j.ceramint.2018.09.116

15. P. Samadipakchin, H. R. Mortaheb, and A. Zolfaghari, *J. Photochem. Photobiol. A. Chem.* 337, 91 (**2017**).

16. A. Umar, H. Algarni, S. H. Kim, and M. S. Al-Assiri, *Ceram. Int.* 42, 13215 (**2016**).

17. H-K. Seo, and H-S. Shin, *Mater. Lett.* 159, 265 (**2015**).

18. Z. Zheng, X. Li, L. Li, and Y. Tang, *Int. J. Hydrogen. Energy*. (2018), https://doi.org/10.1016/j.ijhydene.2018.06.150

19. D. Byrne, E. McGlynn, K. Kumar, M. Biswas, M. O. Henry, and G. Hughes, *Cryst. Growth. Des.* 10, 2400 (**2010**).

20. E. S. Babu, S. Kim, J.-H. Song, and S-K. Hong, *Chem.* Phys. *Lett*. 658, 182 (**2016**).

585 21. Z. Ye, T. Wang, S. Wu, X. Ji, and Q. Zhang, *J. Alloys. Compd.* 690, 189 (**2017**).

586

587 22. D. Byrne, E. McGlynn, M. O. Henry, K. Kumar and G. Hughes, *Thin Solid Films* 518,

588 4489 (**2010**).

589

590 23. T. Wanotayan, J. Panpranot, J. and Qin, Y. Boonyongmaneerat, *Mater. Sci. Semicond.*

591 *Process.* 74, 232 (**2018**).

592

593 24. P. Khamkhoma, S. Pokai, C. Chananonnawathorn, M. Horprathum, P. Eiamchai, V.

594 Pattantsetakul, S. Limwichean, N. Nuntawong, P. Limnonthakul, and J. Kaewkhao,

595 *Mater. Today. Proc.* 5, 14121 (**2018**).

596

597 25. M. Poornajar, P. Marashi, D.H. Fatmehsari, and M.K. Esfahani, *Ceram. Int.* 42, 173

598 (**2016**).

599

600 26. P. K. Baviskar, P. R. Nikam, S. S. Gargote, A. Ennaoui, and B. R. Sankapal. *J. Alloys.*

601 *Compd.* 551, 233 (**2013**).

602

603 27. I. Sirés, E. Brillas, M. A. Oturan, M. A. Rodrigo, and M. Panizza, *Environ. Sci. Pollut.*

604 *Res.* 21, 8336 (**2014**).

605

606 28. S. Garcia-Segura, and E. Brillas, J. Photochem. Photobiol., C. 31, 1, (**2017**).

607

608 29. D. Cao, Y. Wang, and X. Zhao, *Curr. Opin. Green. Sustain. Chem.* 6, 78, (**2017**).

609

30. S. Han, W. Qu, J. Xu, D. Wu, Z. Shi, Z. Wen, Y. Tian, and X. Li, *Phys. Status. Solidi. A.* 214, 1700059 (**2017**).

31. D. Liu, C. Guo, S. Liu, B. Yang, and Z. Jiang, *J. Nanosci. Nanotechnol.* 16, 8308 (**2016**).

32. C. J. Lin, S-J. Liao, L-C. Kao, and S. Y. H. Liou, *J. Hazard. Mater.* 291, 9, (**2015**).

33. R. D. Suryavanshi, S. V. Mohite, A. A. Bagade, S. K. Shaikh, J. B. Thorat, and K. Y. Rajpure, *Mater. Res. Bull.* 101, 324 (**2018**).

34. Z. Sarwar, M. Ashraf, A. Rehman, H. Aziz, A. Javid, N. Nasir, K. Iqbal, T. Hussain, and A. Ashar, *J. Clean. Prod.* 201, 909 (**2018**).

35. N. T. Hoa, V. V. Cuong, and N. D. Lam. *Mater. Chem. Phys.* 204, 397 (**2018**).

36. Y. Zeng, X. Chen, Z. Yi, Y. Yi, and X. Xu, *Appl. Surf. Sci.* 441, 40 (**2018**).

37. C.G. Hatchard, and C.A. Parker, *Proc. R. Soc. A.* 235, 518 (**1956**).

38. W. Maryam, N. Fazrina, M. R. Hashim, H. C. Hsu, and M. M. Halim. *Photonics. Nanostruct.* 26, 52 (**2017**).

39. R. T. R. Kumar, E. McGlynn, C. McLoughlin, S. Chakrabarti, R. C. Smith, J. D. Carey, J. P. Mosnier, and M. O. Henry. *Nanotechnology.* 18, 215704 (**2007**).

635 40. Z. S. Hosseini, A. Mortezaali, A. Iraji zad, and S. Fardindoost. *J. Alloys. Compd.* 628,
636 222 (**2015**).
637
638 41. T-h. Lee, H. Ryu, and W-J. Lee. *J. Alloys. Compd.* 597, 85 (**2014**).
639
640 42. A. D. Mauro, M. E. Fragalà, V. Privitera, and G. Impellizzeri. *Mater. Sci. Semicond.*
641 *Process.* 69, 44 (*2017*).
642
643 43. G. Meng, X. Fang, Y. Zhou, J. Seo, W. Dong, S. Hasegawa, H. Asahi, Hiroyuki
644 Tambo, M. Kong, and L. Li. *J. Alloys. Compd.* 491, 72 (**2010**).
645
646 44. I. Udom, M. K. Ram, E. K. Stefanakos, A. F. Hepp, and D. Y. Goswami, *Mater. Sci.*
647 *Semicond. Process.* 16, 2070, (**2013**).
648
649 45. C. Gray, J. Cullen, C. Byrne, G. Hughes, I. Buyanova, W. Chen, M. O. Henry, and E.
650 McGlynn, *J Cryst. Growth.* 429, 6 (**2015**).
651
652 46. E. McCarthy, R. T. R. Kumar, B. Doggett, S. Chakrabarti, R. J. O'Haire, S. B.
653 Newcomb, J-P. Mosnier, M. O. Henry, and E. McGlynn, *J. Phys. D: Appl. Phys.* 44,
654 375401 (2011).
655
656 47. A. Taurino, M. Catalano, A. Cretì, M. Lomascolo, C. Martucci, and F. Quaranta,
657 *Mater. Sci. Eng.* 172, 225 (**2010**).
658
659 48. B-H. Hwang, *J. Phys. D: Appl. Phys.* 34, 2469 (**2001**).

660 49. R. T. R. Kumar, E. McGlynn, M. Biswas, R. Saunders, G. Trolliard, B. Soulestin, J.-
661 R. Duclere, J. P. Mosnier, and M. O. Henry. *J. Appl. Phys.* 104, 084309-1 (**2008**).
662
663 50. C. A. Jaramillo-Páez, J. A. Navío, M. C. Hidalgo, and M. Macías, *Catal. Today*. 313
664 12 (**2018**).
665
666 51. N. Jia, X. Wang, H-g. Wang, M. Zhang, and M. Guo. *Ceram. Int.* 42, 18459 (**2016**).
667
668 52. C. M. Mbulanga, Z. N. Urgessa, S. R. T. Djiokap, J. R. Botha, M. M. Duvenhage, and
669 H. C. Swart. *Physica B.* 480, 42 (**2016**).
670
671 53. B. S. Mwankemwa, F. J. Nambala, F. Kyeyune, T. T. Hlatshwayo, J. M. Nel, and M.
672 Diale. *Mater. Sci. Semicond. Process.* 71, 209 (**2017**).
673
674 54. Y. Caglar, M. Caglar, S. Ilican. *Optik* 164, 424 (**2018**).
675
676 55. P.-T. Hsieh, Y.-C. Chien, K.-S. Kao, and C.-M. Wang. *Appl. Phys. A.* 90, 317 (**2008**).
677
678 56. S. Ilican. *J. Alloys. Compd.* 553, 225 (**2013**).
679
680 57. W-C. Huang, J. L. Chiu, X. D. Lin, Y. C. Lin, S. C. Tsai, W. M. Su, C. Y. Weng, C.
681 C. Lu, C. F. Lin, and H. Chen. *Results in Physics*. 10, 132 (**2018**).
682
683 58. A. Ali, G. Rahman, T. Ali, M. Nadeem, S. K. Hasanain, and M. Sultan. *Physica. E.*
684 *Low. Dimens. Syst. Nanostruct.* 103, 329 (**2018**).

685 59. E. Velayi, and R. Norouzbeigi. *Appl. Surf. Sci.* 441, 156 (**2018**).

686

687 60. S. Duo, R. Zhong, Z. Liu, J. Wang, T. Liu, C. Huang, and H. Wu. *J. Phys. Chem.*

688 *Solids.* 120, 20 (**2018**).

689

690 61. H.Y. Erbil. *Surf. Sci. Rep.* 69, 325 (**2014**).

691

692 62. D. Byrne, R. F. Allah, T. Ben, D. G. Robledo, B. Twamley, M. O. Henry, and E.

693 McGlynn. *Cryst. Growth. Des.* 11, 5378 (**2011**).

694

695 63. S. Radhika., and J. Thomas. *J. Environ. Chem. Eng.* 5, 4239 (**2017**).

696